INTERNATIONAL JOURNAL OF HYDROGEN ENERGY 47 (2022) 30347–30358

Available online at www.sciencedirect.com

ScienceDirect

journal homepage: www.elsevier.com/locate/he

Performance assessment of a low-cost, scalable 0.5 kW alkaline zero-gap electrolyser

William J.F. Gannon[*], *Maximillian Newberry*, *Charles W. Dunnill*

Energy Safety Research Institute, Swansea University, SA1 8EN, UK

HIGHLIGHTS

- 84% efficient at 65 °C and 400 mA/cm^2. Cell voltage still below 2 V at 800 mA/cm^2.
- Simplified flowplate that makes use of spot-welding to eliminate machining costs.
- Total material cost to build a 0.5 kW electrolyser is under 50 GBP (70 USD).

GRAPHICAL ABSTRACT

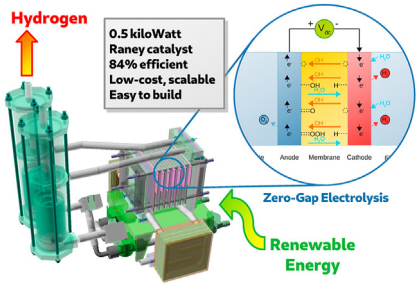

ARTICLE INFO

Article history:
Received 10 December 2021
Received in revised form
20 May 2022
Accepted 4 July 2022
Available online 19 August 2022

Keywords:
Alkaline electrolysis
Water-splitting
Zero-gap
Hydrogen

ABSTRACT

The performance of a six-cell zero-gap electrolyser with an active area of 300 cm^2 was analysed. The device featured a new design of flowplate that employed spot-welding in order to eliminate machining costs. Direct resistance measurements were made, and computer simulations performed to confirm the sub milli-ohm resistance of the flowplate design. An electrolyser test-rig was constructed to permit performance characterisation with various electrolytes and membranes at varying temperatures, and versus a comparable finite-gap design. The results were fitted to a simplified four-parameter model which permitted quantitative comparison, and performance projection up to a 100 kW device. The highest performance achieved was 84% efficiency with 6 M KOH at 65 °C and 400 mA/cm^2, and the cell voltage was still below 2 V at 800 mA/cm^2. The total material cost to build a 0.5 kW electrolyser is under 50 GBP (70 USD).

* *Corresponding author.*
E-mail address: esri@swansea.ac.uk (W.J.F. Gannon).

https://doi.org/10.1016/j.ijhydene.2022.07.040

Introduction

The use of renewable energy to split water into hydrogen and oxygen is a crucial part of a future de-carbonised, climate neutral society [6,9,10]. Although various methods exist to do this, the use of green electricity with an electrolyser is the simplest and by far the most widespread [49]. In a conventional Finite-Gap Electrolyser (FGE) electricity is conducted from anode to cathode through an electrolyte fitted with a gas-separation membrane, to produce the sequence "anode | electrolyte | membrane | electrolyte | cathode" [36,41]. In a Zero-gap Electrolyser (ZGE) this order is rearranged as far as possible to become "electrolyte | anode | membrane | cathode | electrolyte", as shown in Fig. 1 [8,37,39]. As a result the ohmic losses in the electrolyte are minimised, but at the expense that the electrode must transport not only electrons, but also be porous to both electrolyte and gaseous products [38]. A highly congested region is thereby created where compromises must be made, trading off one aspect of performance against another.

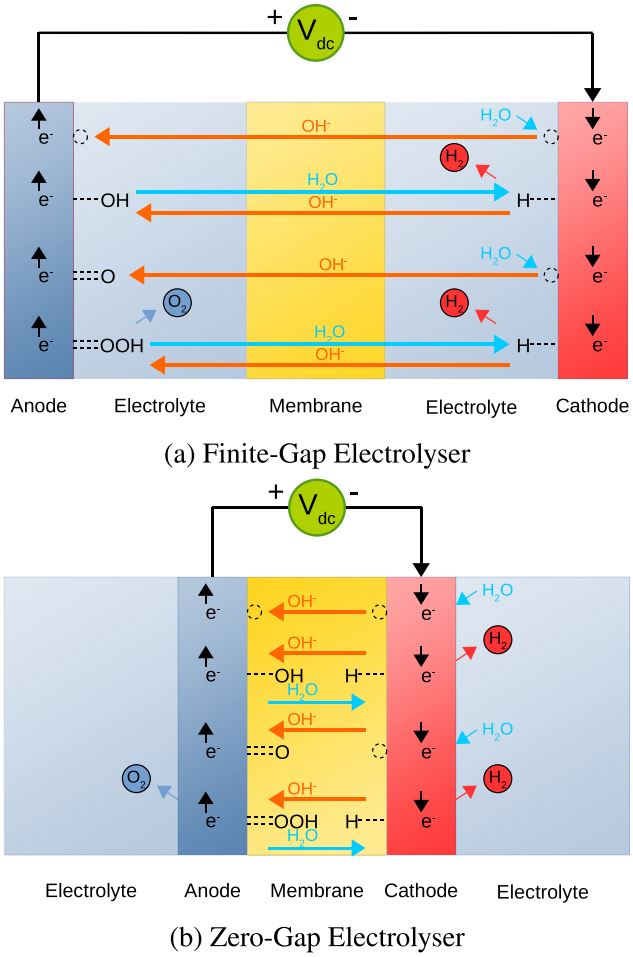

Fig. 1 – FGE and ZGE Electrolyser configurations. The diagram shows the adsorbed species typical for a 4-electron Oxygen Evolution Reaction and 2-electron Hydrogen Evolution Reaction in alkaline conditions. Note that both OH^- ions and water must pass through the membrane.

Other reconfigurations have been investigated, for example Divergent Electrode Flow Through (DEFT), where a continuous flow of electrolyte is maintained through the electrodes, so that gaseous products are swept away without mixing, and no membrane is required [18]. Another variation is the Rotating Electrolyser, whereby rotating disks induce 'wall jets' that maintain product separation, also without the need for a membrane [26]. However, these configurations remain the exception rather than the rule, and a gas-separation membrane is an important part of nearly all modern electrolysers.

Alkaline zero-gap electrolysers have achieved impressive results, some of which are comparable with proton-exchange membrane based on an acidic environment. In 2017 Phillips et al. achieved a cell voltage of 3.05 V at 500 mA cm^{-2} with 1 M NaOH at laboratory temperature, with electrodes made of 40 tpi woven stainless-steel mesh with no catalytic coating [38]. The device had an active area of 10 cm^2, and used a Zirfon membrane. Haverkort et al. achieved a voltage of 2.5 V at 1 A cm^{-2} with 6 M KOH at 300 K, with electrodes made of perforated metal with Ru and nickel oxide catalysts [24]. The device had an active area of 10 cm^2, and used a Zirfon membrane. Schalenbach et al. measured a cell voltage of 1.85 V at 2 A cm^{-2} with 30 wt% KOH at 80 °C, using nickel mesh electrodes manufactured using metallurgical hot dip galvanisation [45]. The device had an active area of 9 cm^2, milled solid nickel flow fields, and a polyethersulfone membrane. No performance variation with temperature was investigated.

Studies into the performance of electrolyser design typically involve an active area of a few square centimetres [45]. Whilst this is enough to obtain indicative and often impressive results, it is wrong to assume that such results can be scaled. This study aims to investigate this scalability using a device with an active area of 300 cm^2. One problem is the amount of gas produced at high current densities. An electrolyser passing 1 A cm^{-2} at atmospheric pressure is awash with evolved gas, and the larger the surface area, the more problematic this becomes. It is known that the resistivity of an electrolyte increases as a function of the void fraction of gas within it, in accordance with the Bruggeman equation $\rho = \rho_0(1-f)^{-3/2}$, where f is the void fraction and ρ_0 is the quiescent electrolyte resistivity [27,32,48]. Since gas is evolved at an almost constant rate across the face of the electrode, the quantity of gas increases in the direction of electrolyte travel. As a result, at the point where the current density is sufficient to fill 50% of the electrolyte with bubbles, the resistivity of the electrolyte is *tripled*. Similarly, the greater the stack length, the more the issue of gas discharge is compounded, based on the assumption that the gas must exit from the ends of the stack. As a result, studies that analyse the performance of electrolysers with larger areas and stack lengths are useful additions to the literature.

A zero-gap electrolyser has the advantage that there are no bubble curtains between the electrodes, however gas is still evolved within the microscopic structure of the porous electrodes, and nanobubbles can form inside the membrane [21]. In fact, some authors go further and state that much of the surface of the electrode facing the membrane is inactive due to gas coverage, and that a gap of 0.2 mm should be

deliberately introduced to mitigate this, thereby suggesting that optimum zero-gap electrolysis is not achieved with a zero gap [24]. This clearly highlights the risk of creating locally stagnant conditions, where electrolyte inflow and gas outflow cannot meet the demands of the electrochemical reaction. Perhaps more seriously, the constrained evolution of gas could produce a localised overpressure, forcing gas into the membrane and increasing gas cross-over [31].

This situation can be alleviated by operating the electrolyser at elevated pressure, such that the volume of gas is reduced, and most commercial electrolysers operate between 10 and 30 bar [49]. However, there are compelling reasons not to operate an electrolyser significantly above atmospheric pressure. First is that it increases the cost and complexity of electrolyser construction, since it is harder to prevent leaks. This vulnerability is exacerbated by repeated pressure cycling, which is an inevitable consequence of renewable energy applications. A pressurised electrolyser must be de-pressurised during idle periods, otherwise a high-pressure explosive mixture is generated due to the diffusion of dissolved gases [5]. Subsequently, the start-up delay of the electrolyser during re-pressurisation and self-test can take many minutes, further reducing the ability to follow the peaks and troughs of rapidly fluctuating power sources. Worse still, commercial electrolysers specifying a maximum number of shut-down-start-up cycles will see a drastic reduction in service life [50]. An ambient-temperature, atmospheric-pressure electrolyser never needs to be de-pressurised, and has no start-up delay [10].

The regulations surrounding the transport and storage of pressurised hydrogen increase cost and complexity, which slow the roll-out of hydrogen technology and limit its feasibility [25,33,56]. Liquid Organic Hydrogen Carriers (LOHCs) such as ammonia and Dibenzyltoluene are an alternative method of hydrogen storage which do not involve high-pressure gas storage [40]. However, they must contend with other problems, such as toxicity to humans along with high energy losses and costly catalyst decay associated with the hydrogenation and dehydrogenation of the carrier [42]. Batteries exhibit much higher electrical energy storage efficiencies along with decreased system complexity, but are a less versatile fuel source with limited long term storage capabilities [35]. In other cases adopting an immediate consumption strategy with zero storage can overcome storage complexity whilst also permitting the use of HHO, i.e. the stoichiometric mixture of hydrogen and oxygen that is produced with no gas membranes [47].Where hydrogen gas is to be stored, there are some advantages to doing so at a pressure less than 0.5 bar above atmospheric. Although this uses more volume, it is subject to fewer regulations since at least in Europe (according to European Pressure Equipment Directive 2014/68/EU) it is not classified as a pressure vessel. For applications where size is not an issue, at this pressure each kilogram of H_2 occupies 8 m^3, which is the same as the largest commonly available hydrogen gas cylinder (size K) at 277 bar. Should a leak occur, the positive pressure prevents the ingress of atmospheric air, as well as providing drive pressure for transportation along pipes. In addition to hydrogen sensors [54], a passive autocatalytic recombiner (PAR) can act as a further safeguard to eliminate as far as possible the explosion risk [3,4]. Such a storage system is optimised to work with a low-pressure electrolyser, since there is little point in pressurising the gas just to de-pressurise it again for storage.

Many studies into zero-gap electrolyser design make use of flow-fields which have been machined from solid metal [38,45]. Whilst there is no doubting their performance, it is worth questioning whether they can be produced more cost-effectively. Notwithstanding the cost of raw material, 316-grade stainless steel is a difficult material to machine, achieving an American Iron and Steel Institute (AISI) Machinability Rating of just 45%.[1] This is one of the lowest ratings for any steel that isn't a tool steel, i.e. a steel that is used to cut steel. As such, the machining of flow-fields adds significant cost, both in terms of time and tool degradation.

Materials and method

Leakage currents

Electrical power is more easily transported at higher voltage and lower current. This minimises not just ohmic losses, but also the expense of high current electrical conductors, safety equipment and switch gear. The standard output of a commercial wind turbine is 690 V [17], which derives from the operating voltage in Europe (400 V 3-phase) multiplied by the square root of three. After rectification, this is still much higher than the typical input voltage of an electrolyser. A bipolar electrolyser is able to partially bridge this gap, since it operates at higher voltage and lower current than a unipolar design. However, a serious disadvantage of a bipolar design is that leakage currents flow wherever cells operating at differing voltages are connected via side-channels [28,44]. The leakage currents do not just reduce the efficiency of the electrolyser, but can lead to polarity inversion, whereby a portion of an anode becomes cathodic or *vice versa* [29]. This in turn leads to greater corrosion and electrode damage, but also to potentially explosive gas-mixing. It is theorised that such mixing could have been a contributory factor to the lethal explosion of an electrolyser in 1975 [29].

The six cell design here presented is a development of a previous single-cell design that achieved a voltage of 2.47 V at 500 mA cm^{-2} with 1 M NaOH at 70 °C. It was constructed using unconductive laser-engraved acrylic flowfields and a Zirfon membrane. The Faradaic efficiency was confirmed to be at least 98%, and the crossover of O_2 into H_2 with 0.5 M NaOH at 250 mA cm^{-2} was 1.24% [14]. The new six-cell design features three independent routes through the stack for inlet and outlet electrolyte flows. As such, nowhere are more than two adjacent cells joined by the shortest side-channels of the lowest-resistance. For widely-separated cells, the connecting route via the ends of the stack is of much greater length, and thus the leakage currents reduced. This is shown diagrammatically in Fig. 2.

Fig. 2(a) shows a six-cell zero-gap electrolyser with two channels straight through the stack for the electrolyte inlet and outlet (for simplicity, only the hydrogen circuit is shown). The

[1] Source: https://www.engineeringtoolbox.com/machinability-metals-d_1450.html viewed May 2022.

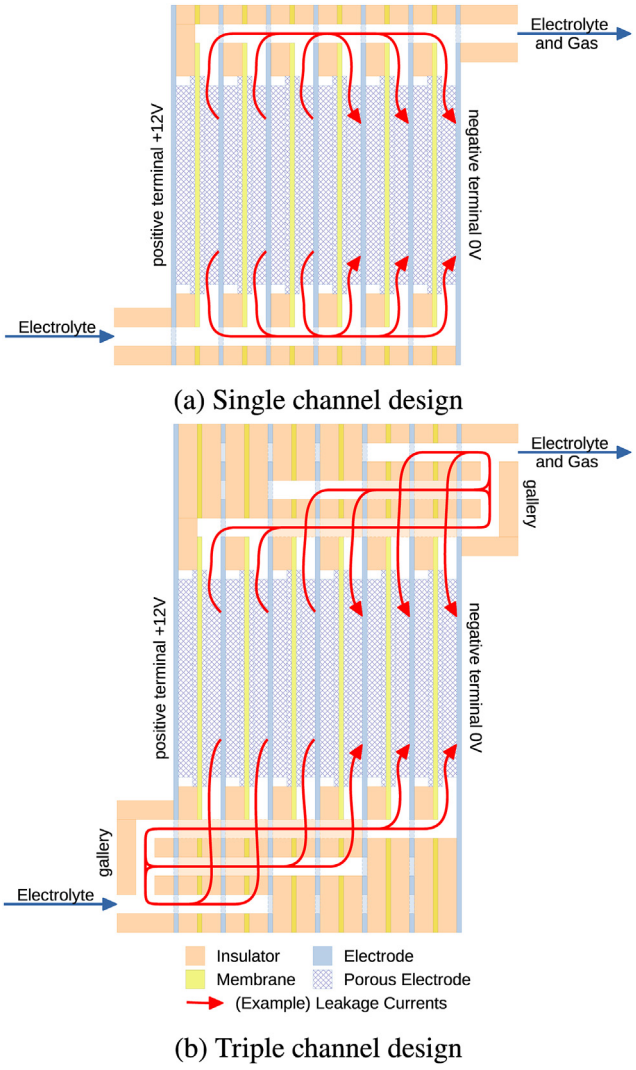

Fig. 2 – Leakage currents in a six-cell bipolar zero-gap electrolyser. By altering the design to incorporate multiple parallel paths, leakage currents can be reduced.

red lines show some of the many possible leakage current paths, which will exist between any two metal surfaces with potentials that differ by more than 1.23 V. Even though the cross-sectional area of the channels is small, the potential difference across them is high (i.e. more than 12 V). Therefore, since electrical heat dissipation is equal to V^2/R, a modest amount of conductance can produce a significant loss of performance. The losses are realised as self-heating, not as Faradaic inefficiency, and cause slightly more hydrogen to be evolved at the cathodic end of the stack than at the anodic end.

Fig. 2(b) shows the same electrolyser redesigned to incorporate 3 parallel circuits through the stack, each serving two adjacent cells. Note in practice that the circuits are not stacked vertically as shown, but spread across the top and bottom surfaces of the electrolyser (see the SI for scale drawings). With the new design, the conductive path between electrodes with widely differing potentials can occur only via the galleries at each end of the stack. Since a longer path has greater resistance, leakage currents are reduced. The more complex design adds little to the total cost of the electrolyser, and has the additional benefit that electrolyte pumping resistance is reduced.

The currents can be calculated using Kirchoff's laws, and in general show that percentage losses increase *linearly* with the number of cells [28]. Thus, for any mitigation scheme it is expected that a maximum stack-length will be reached where the losses are too great. For the design here presented it is estimated this will occur somewhere between 25 and 50 cells. For greater stack lengths, inlet and outlet electrolyte flows can be designed to incorporate air-gaps.

Flowplate

The task of the flowplate is to support the electrodes in contact with the gas-separation membrane, with a mixture of electrolyte and gas behind. The electrical resistance of the flowplate is critical to the performance of the electrolyser, since at a current density of 1 A cm^{-2} a resistance of just 0.1 Ω cm^2 (per side) results in an additional voltage of 200 mV per cell. This alone is sufficient to reduce the voltage efficiency of the electrolyser by 12%. For the electrolyser design here presented, which has an active area of 50.8 cm^2, this equates to a maximum permissible resistance of just 2 mΩ per side, and ideally much less.

The metal components of the electrolyser were constructed using 316-grade stainless steel, since it is a widely available, relatively low-cost material, and has high chemical resistance. A perforated version with 3 mm holes was chosen for the backing plate, which sits immediately behind the electrodes. The 0.9 mm mid-plate had a measured electrical resistance of 0.6 mΩ per square, which tallies with the published bulk resistivity of 6.9×10^{-7} Ω m, from which a figure of 0.77 mΩ/□ is predicted.[2] By contrast, the perforated sheet had a measured resistance of 2 mΩ/□. Based on the maximum permissible resistance above, it was clear that the flowplate had to be designed such that no part of it presented an electrical resistance of 'more than one square' of the perforated sheet.

It is difficult to envisage this in practice, therefore an experiment was conducted to directly measure the conductance of the flowplate. This was performed using a Circuit-Specialists.eu CSI 3060SW 60 A power-supply, plus a multimeter. A single-sided flowplate, backed by an 8 mm mild-steel plate was attached to one terminal of the power-supply and multimeter. The other terminal was bolted ~5 mm from the corner of a piece of 0.9 mm 316-grade stainless-steel sheet. It was discovered that it was not possible to produce a reliable contact using pressure alone. However, with the power-supply set almost to zero, it was found that touching the corner of the sheet to the surface of the flowplate would cause it to be temporarily welded in place. The current could then be increased to 10 A to obtain a voltage reading from the multimeter. At this current a resistance of 1 mΩ generates a voltage of 10 mV, which is within the measurable range of a standard multimeter.

In addition, a model was built of the flowplate in SolidWorks™, which is a 3D CAD software package with finite element analysis, with heat-flow being used to model the

[2] source: https://www.thoughtco.com/table-of-electrical-resistivity-conductivity-608499 viewed May 2022.

electrical resistance. This works because the steady-state solution of the heat equation is completely analogous to Ohm's law, a situation that is well understood and even known to apply to transient phenomena [53]. The arrival and departure of the heat flux was constrained to specific areas of the flowplate using two cylindrical rods of diameter 6 mm, which therefore emulated the point-to-point resistance measurement that is obtained using a multimeter. In this way it was possible to map how the electrical resistance varied across the surface of the flowplate, and thus to determine where improvements could be made. The results obtained are as presented in Section Flowplate resistance simulation.

In practice, measuring the point-to-point resistance of the flowplate does not accurately represent its performance. This is because the current is constrained to flow down each of the metal spacers, which act as bottle-necks. As a result, some of the current will take the shorter, but higher resistance route directly through the electrolyte, thereby partially performing more like a finite-gap electrolyser. Neither is the current available at each point on the electrode unconstrained, since it is dependent on the supply and removal of chemical species to the catalytic reaction surfaces. These in turn are utilised in accordance with the non-linear Butler-Volmer dependence of the rate of reaction on the voltage at each point of the electrode. The only accurate method to model each of these interactions is with a multi-physics simulation, however this was felt to be beyond the scope of this study.

Electrodes

The electrodes were constructed of 40 thread-per-inch woven 304-grade stainless-steel mesh. This was chosen to present a low-cost framework that was strong and could be spot-welded into place. The spot-welder chosen was a battery powered USB-rechargeable device with a maximum output current of 649 A. The spot-welder can apply two spot-welds every 1.5 s, and approximately 200 small spot-welds were used per electrode. After assembly, a Raney 2.0 catalytic coating was applied to the electrodes, as described in previous publications [12,13,15]. The same catalyst was used for both anode and cathode, since the coating is an acceptable bifunctional catalyst. To further reduce costs, the coating could be omitted from the anodes, since stainless-steel is known to operate as an efficient electrocatalyst by itself [55].

Membrane

Two different membrane materials were tested, those being Zirfon™ and Polyethersulphone (PES). Zirfon is a hydrophilic membrane constructed of zirconium oxide powder stabilised onto a polysulphone matrix. The stability of the ZrO_2 to extreme alkaline and high temperature conditions makes it a reliable choice, however more recent membrane materials are able to outperform it in terms of electrical resistance, for example Sustainion [34], Fumasep [30] and IMET [20]. However, these materials remain prohibitively expensive, and can be subject to non-commercial use agreements. Surprisingly, an even cheaper but still effective material is woven stainless steel mesh [16], but as an electrically conductive material is unsuitable for zero-gap electrolysis without modification.

The PES membrane (Sterlitech PES022005) is a commercially available filtration material with a pore size of 0.2 μm. It is known to be stable for use in alkaline electrolysis [45]. It has been modified for use as an anion exchange membrane [52]. The hydrophobic nature of unmodified PES may make it a poor choice for gas-separation, which would need to be confirmed in future experiments that assess gas-mixing.

Direct measurements of the membrane area resistance were made using a separate two-electrode test-cell constructed from laser-cut acrylic. Measurements were taken with and without the membrane, and the resistance calculated as the difference of the two. The electrodes were made from 316-grade stainless steel, the exposed area of the membrane was 36 cm^2, and the electrolyte was 30 wt% KOH at laboratory temperature. All impedances were measured using Electrochemical Impedance Spectroscopy between 0.1 Hz and 10 kHz at 100 mV on an Ivium n-Stat potentiostat. The resistance of the cell was calculated from the projected intercept of the Nyquist plot with the x-axis at high frequency.

Construction

The most widespread method of joining stainless steel is welding, although soldering and brazing are possible [2]. However, stainless steel is regarded as a challenging material to weld, distorting easily when heated, and conducting less heat away than regular steel. More seriously welding and brazing can introduce unwanted elements, such as copper, and soldering introduces tin, which dissolves in NaOH/KOH. Copper is leached out by electrolysis and deposited on the cathode, thereby potentially inhibiting the hydrogen evolution catalyst [12]. Nevertheless, it is possible to weld stainless steel without introducing foreign material using electrical spot-welding.

The spot-welder chosen was a Sealey SR123 capable of delivering up to 6300 A. Although spot-welding works best when restricted to joining two parallel pieces of sheet metal, it was discovered that it is possible to join up to three pieces of metal at right angles, i.e. to form two butt welds. This was achieved by filing 2 mm-wide grooves into the ends of the copper prongs of the spot-welder. It was therefore possible to construct a flowplate with sizeable 2 mm ribs to keep electrical resistance down. A metal frame was required to prevent large amounts of distortion. In addition, to maintain planarity of the flowplate the ribs and backing plates were filed by hand after each step. The finished design of flowplate is as shown in Fig. 3(a), and as described in greater detail in the SI.

Electrolyser Test Station

In order to test the electrolyser over a range of temperatures and flow-rates, a test-station was constructed, as shown in Fig. 3(b). A pair of multi-layer heat-exchangers were used to heat the electrolyte, themselves heated by hot-water (not shown). This was sufficient to heat the electrolyte to ~70 °C without boiling the heating water. The temperature was measured using temperature loggers (Elitech RC-4), with

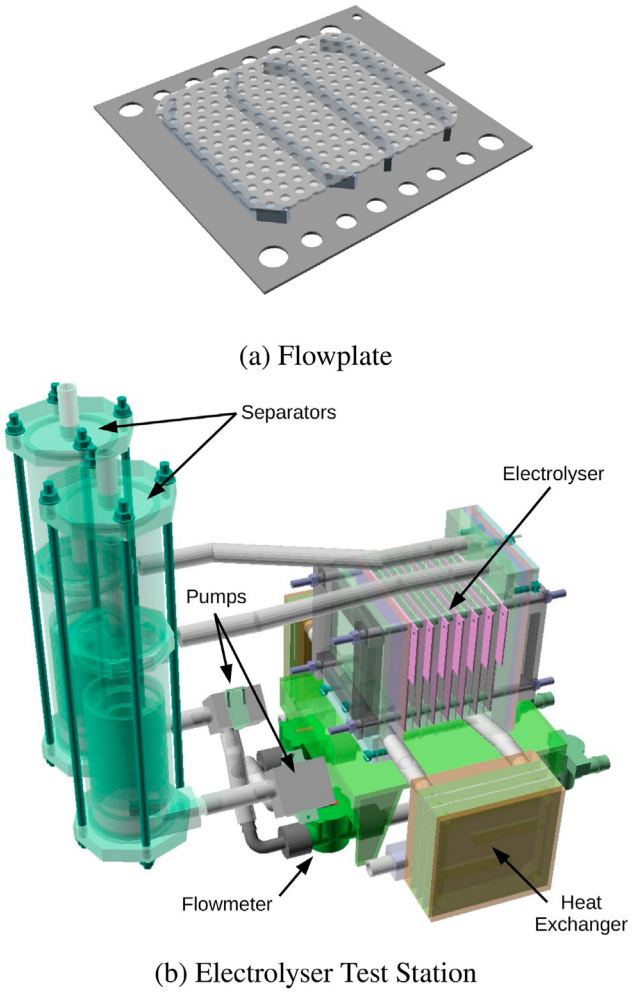

Fig. 3 – Flowplate and Test Station. Images produced using OpenScad.

external probes inserted directly into the inlet and outlet galleries of the electrolyser. The recorded temperature was an average of the two readings, to compensate for self-heating.

Two separate bodies of electrolyte were maintained, with no external mixing, although levels were free to equalise through the membranes. This was primarily to prevent cross-contamination from anode to cathode and *vice versa* as has been observed [11], although it has been shown this can lead to hydroxide ion depletion of the anolyte [22,23]. Electrolyte circulation was controlled using two brushless d.c. pumps, and measured using Hall-effect inline flowmeters (model DN15), which generate one pulse for each 2.25 ml of flow, the pulses being counted and timed by an Arduino. The flowrate for each body of electrolyte was typically around 24 ml s^{-1}

The mixture of gas and liquid leaving the electrolyser was treated using a vortex separator, constructed using laser-cut acrylic components. This reduced the total volume of electrolyte, making it less time-consuming to change temperature.

The evolved gases were vented to the atmosphere, however in future versions it would be beneficial to measure the volumes produced. This is particularly relevant at low current densities where the stack voltage falls far below the thermoneutral voltage 8.88 V. This occurs because the cells progressively 'switch off', with current conduction occurring via side-channels, an effect which could be assessed by measuring the Faradaic efficiency.

Results

Membrane resistance measurement

The area resistance of the Zirfon and PES membranes was measured using the procedure described in Section Membrane, with the results as presented in Table 1. The results show that at high frequency the PES membrane presented an area resistance of 724 μΩ m^2, whereas the resistance of the Zirfon membrane was much lower at 47 μΩ m^2. However, these results should be treated with caution, since an electrolyser operates with direct current and a high-frequency resistance measurement is not necessarily applicable. Nevertheless, they do serve to highlight the high level of porosity of the Zirfon membrane, as previously studied [51].

Flowplate resistance measurement

The resistance of the flowplate was measured using the procedure described in Section Flowplate. A total of 16 point readings were taken. Many potential sources of inaccuracy existed, therefore the results were not expected to be more than 'confirmatory'. One notable problem was that the welded connection was not repeatable. Another was that the corner of the plate was gradually burnt away, such that the distance between the multimeter probe and the flowplate surface gradually reduced. This made it impossible to obtain accurate sub milli-ohm resistance readings. Nevertheless, the results were sufficient to confirm that the resistance of the plate appeared to be 'about 1 mΩ'. It was therefore decided to simulate the resistance using software.

Flowplate resistance simulation

The results of the simulation in SolidWorks™ of the flowplate electrical resistance were as presented in Fig. 4. A total of 24 simulations were conducted at different points within one quadrant of the backing plate. Using symmetry, these were then reflected to generate 96 datapoints, and interpolation employed to generate an image.

The results show that the calculated resistance varied between 0.29 and 0.97 mΩ, which therefore comfortably achieved the desirable design criterion of 'no more than 2 mΩ per

Table 1 – Resistance measurements of the Zirfon and PES membranes.

Membrane	None	Zirfon	PES
Electrode Gap (mm)	26.24	26.87	26.40
Resistance Intercept (Ω)	0.163	0.177	0.364
Net Resistance (Ω)	–	0.013	0.201
Area Resistance (μΩ m^2)	–	47	724

side' (see Section Flowplate). The average resistance was 0.58 mΩ, which equates to 0.29 mΩ per side, although electrolyser performance is not expected to be as good as this due to congestion effects. The lowest electrical resistance occurred above the spacing ribs, since these provide the most direct electrical connection. Likewise the highest resistance occurred on the top and bottom edges, providing valuable guidance to inform future design iterations.

Zero-gap versus finite-gap

The results of a direct comparison between the performance of the Finite-gap (FGE) and Zero-gap (ZGE) electrolysers are as shown in Fig. 5.

The results show that the ZGE outperformed the FGE in all circumstances, producing a reduction in stack voltage of up to 4 V, which is sufficient to increase the efficiency of the stack from 55% to 73% at 400 mA cm^{-2}. At the highest temperature, and a current density of 800 mA cm^{-2} (i.e. 40 A) the voltage was still below 12 V, which is 2 V per cell. This is an acceptable value for a device of such low-cost scaled up to dissipate 0.5 kW, and constitutes a voltage efficiency of 75%. At 20 A the efficiency was 84%.

Counter-intuitively, the performance gap between FGE and ZGE was lower with 1 M NaOH than with 6 M KOH, although still obeyed the overall trend. This is surprising, since it might be expected that minimising the gap between electrodes would have more of an effect with lower-conductivity electrolyte. It is possible this is due to the surprisingly high impedance of the gas-separation membrane in less-concentrated electrolyte, an effect which has been observed before [16].

To further investigate this, the effect produced by changing just the membrane from PES to Zirfon was analysed, with the results as presented in Fig. 6(a). The results show that the PES membrane produced a voltage reduction of up to 1.27 V at the highest current density and temperature, although the slope of the I–V curve, which is an indication of the conductivity, was very similar. This reduction was sufficient to reduce the losses due to inefficiency by 23%, rising at 400 mA cm^{-2} to a loss reduction of 31%.

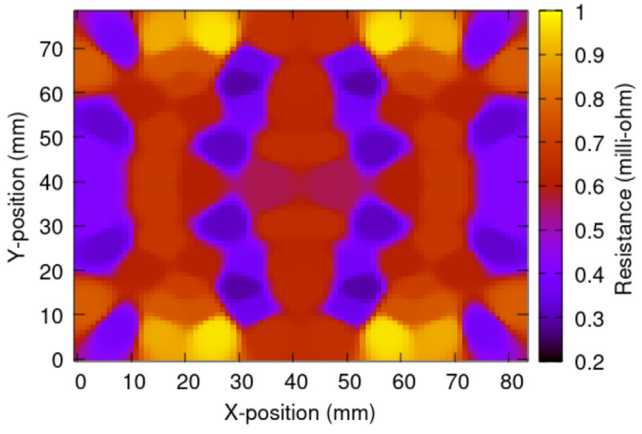

Fig. 4 – Resistance simulation (double-sided).

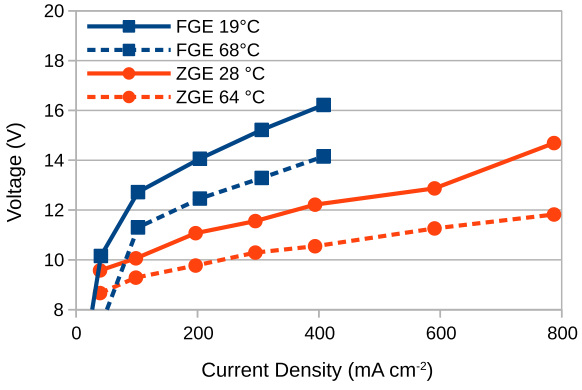

(a) In 6 M KOH

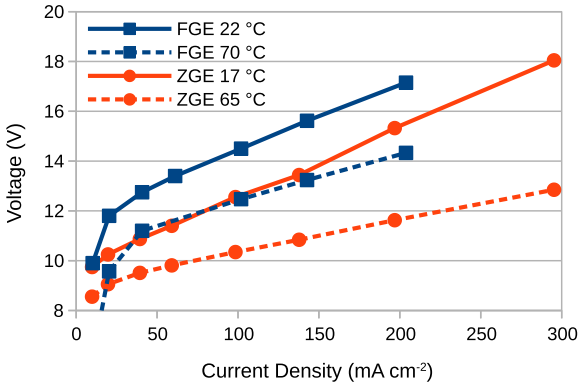

(b) In 1 M NaOH

Fig. 5 – Performance comparisons of ZGE vs FGE, with two different electrolytes.

Model fitting

In an effort to gain further insight into the performance of the ZGE, the results presented in Fig. 5 were fitted to a simple empirical model, as previously described [14]. The model assumes that the electrolyser voltage can be expressed as the sum of three contributions:

$$V_{elect} = V_{therm} + V_{act} + V_{ohmic} \quad (1)$$

$$\text{where} \qquad V_{therm} = V_0 \quad (2)$$

$$V_{act} = b\log(j) \quad (3)$$

$$V_{ohmic} = \frac{j}{(T - T_0)\kappa_0} \quad (4)$$

where V_{therm} is a fixed voltage V_0 that represents the thermodynamics, V_{act} is related to the activation energy and identical in form to the Tafel equation, and V_{ohmic} represents the Ohmic losses. The Ohmic conductance $\kappa = (T - T_0)\kappa_0$ is assumed to be linear with temperature, and to fall to zero at some notional temperature T_0. This is a form observed to be obeyed by electrolytes such as KOH and NaOH [14], and is a first-order simplification of the six variable mixed equation proposed

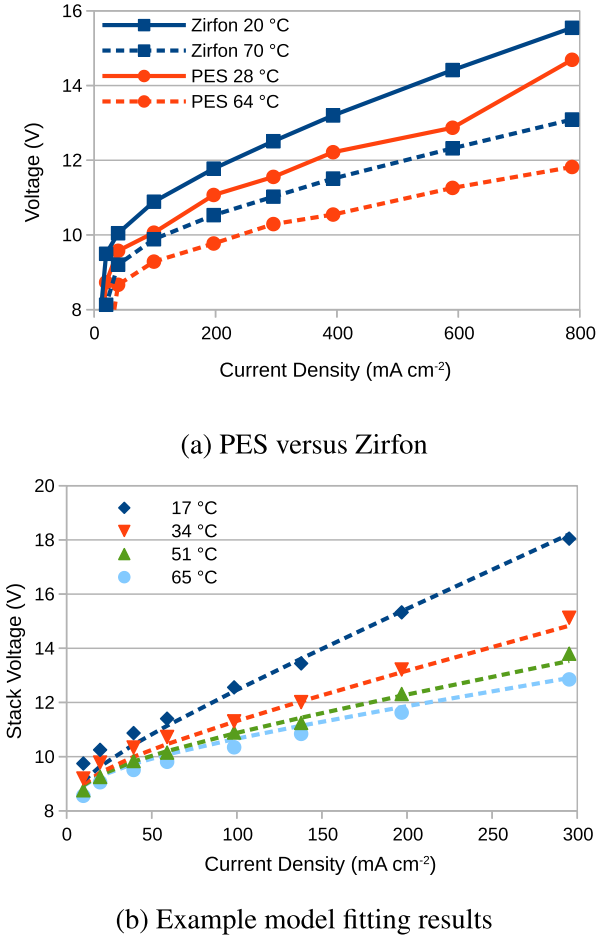

Fig. 6 – a) Performance comparison of PES Membrane versus Zirfon. Configuration: ZGE, Electrolyte: 6 M KOH. b) Model fitting results. Configuration: ZGE, Electrolyte: 1 M NaOH.

Table 2 – Best-fit model parameters for the FGE and ZGE, with two different electrolytes. The values marked with an * have been artificially constrained.

Parameter	1 M NaOH		6 M KOH		
	FGE	ZGE	FGE	ZGE	ZGE
	Zirfon	PES	Zirfon	PES	Zirfon
A (cm^2)	49.1	50.8	49.1	50.8	50.8
V0 (V)	8.58	7.03	8.52	6.57	7.19
b ($V\ dec^{-1}$)	0.9*	0.9*	0.9*	0.9*	0.9*
κ_0 ($S\ K^{-1}\ m^{-2}$)	9.3	14.7	21.8	60.4	51.1
T_0 (K)	259	265	253	271	261
V0 *per cell* (V)	1.43	1.17	1.42	1.10	1.20
κ @ 50 °C ($S\ m^{-2}$)	596	859	1520	3160	3190

Note that in all cases the values below 50 mA cm^{-2} were excluded from the fitting dataset, since the high level of curvature in this region is not explained by the Tafel equation, but instead by some of the cells switching off at low current densities. In practice, this made it difficult to determine the value of parameter b, therefore it was decided to artificially constrain this to 0.9 V dec^{-1}. This equates to 150 mV dec^{-1} per cell, which is the sum of the typical anodic and cathodic Tafel slopes which are expected from theory [46]. A precise value for b is not required, since electrolyser performance above 50 mA cm^{-2} is dominated by the values of the other three parameters.

by Gilliam et al. and which is acceptably accurate over a limited temperature range [19]. When the model fitting was performed, using traditional gradient descent, the values for the FGE and ZGE were as presented in Table 2.

The table also shows parameter V_0 divided by six to obtain the 'thermodynamic voltage per cell'. This varies between 1.10 and 1.20 V for the ZGE, and between 1.42 and 1.43 V for the FGE. In practice, this suggests that the gradient descent has identified that the ZGE produces voltages which are about 0.25 V per cell lower than the FGE, all other things being equal. The values of T_0 imply that the Ohmic conductance of the electrolyser reaches zero at a temperature somewhere below zero celsius. This is not to be taken literally, but is instead a compromise figure that takes into account the temperature dependence of various contributions.

The values of κ_0 and T_0 can be considered together by comparing the projected conductance at 50 °C, as is presented in the bottom row of the table. This shows quantitatively how the conductivity of the electrolyser increases both by changing from finite-gap to zero-gap, and by increasing the concentration of the electrolyte. However, as was confirmed already in Fig. 5, it is notable that the relative increase in performance from FGE to ZGE is not as great in 1 M NaOH as it is in 6 M KOH.

The last two columns are a direct comparison of the PES and Zirfon membranes. They show largely similar figures, but a slight reduction in V_0, which reflects the performance improvement shown in Fig. 6(a). These results are surprising given that the membrane resistance measurements presented in Section Membrane resistance measurement showed that PES had a much higher area resistance at high frequency than Zirfon. It therefore appears that a high-frequency membrane resistance measurement cannot be used to predict the performance of an electrolyser operating at direct current. However, the results do support the findings of Schalenbach et al. who achieved impressive results using PES [45].

An example of the predictions of the model are as shown by the dashed lines in Fig. 6(b).

The dashed lines constitute a reasonable fit to the measured values, but from inspection it is clear that the variation with temperature at lower current densities is greater than that predicted by the model. This implies that some effect is occurring which is *not* proportional to the current density, and therefore cannot be expressed as an Ohmic conductance. For example, this could be due to a reduction in the viscosity of the electrolyte at higher temperatures, but such an effect is not included in the model.

The most important aspect of the model fitting is that it permits different electrolysers to be objectively compared. There is not much (within reason) that can be done to reduce V_{therm} and V_{act}, since they are determined by the laws of physics and the water-splitting reactions at work. But the Ohmic conductance of an electrolyser can be increased by careful design. However, since this is temperature dependent, it is best measured at a common baseline temperature, for example 50 °C. Similarly, since the conductance is inversely

proportional to the number of cells N_C, it should be multiplied by N_C. Therefore, the area and cell-specific conductance of the ZGE here presented in 6 M KOH is:

$$N_C(T - T_0)\kappa_0 = 6 \times (323 - 271) \times 60.4 = 18970\ \text{S cell m}^{-2} = 0.53\ \Omega\ \text{cm}^2\ \text{cell}^{-1}$$

The comparable value for the FGE was 1.1 Ω cm^2 $cell^{-1}$, thus the FGE presented approximately double the resistance of the equivalent zero-gap design. This formula can be used to predict that a ZGE with an active area of 46 cm × 21 cm with 24 cells would present a resistance of 0.53 ÷ 46 ÷ 21 × 24 = 13 mΩ.

With a Zirfon membrane the conductivity figure is slightly higher at 19 140 S cell m^{-2}, although this does not indicate that the membrane is a better material, since the total electrolyser voltage was higher. At 80 °C this equates to a resistivity of 0.35 Ω cm^2 $cell^{-1}$, which is in agreement with figures published by de Groot et al. [21]. It is more difficult to compare with the figure of 0.19 Ω cm^2 $cell^{-1}$ published by Haverkort et al., since the authors have separated the area resistance into two components, one of which scales with electrolyte resistivity.

Electrochemical Impedance Spectroscopy

The Finite and Zero-gap electrolysers were analysed using Electrochemical Impedance Spectroscopy (EIS), with the results as presented in Fig. 7.

The impedance of the electrolyser comprises resistive contributions from the ohmic components (e.g. the metalwork and wiring) and from the electrolyte, as well as capacitive contributions chiefly from the electrodes. The resistance can be determined by measuring or extrapolating the point of intercept of a Nyquist plot with the horizontal axis [7,43], and the capacitance by performing a best-fit with the Bode plot. When this procedure was applied, the values measured were as presented in Table 3.

The results show that the ZGE presented a series ohmic resistance which was 11 times smaller than for the equivalent FGE. This is far greater than the factor of two observed in Section Model fitting, and should be treated with some caution. Using Equation (4) it is possible to use the model fitting parameters from Table 2 to state that:

$$R_{ohmic} = \frac{dV_{ohmic}}{dI} \quad \text{where} \quad I = jA \tag{5}$$

$$\therefore \quad R_{ohmic} = \frac{1}{A(T - T_0)\kappa_0} \tag{6}$$

thus for the ZGE with 6 M KOH at 20 °C the ohmic resistance should be 1 ÷ (0.00508 × (293 − 271) × 60.4) = 146 mΩ, or 1.23 Ω cm^2 $cell^{-1}$ (not to be confused with the figure of 0.35 Ω cm^2 $cell^{-1}$ from Section Model fitting, which was calculated for 80 °C). The ZGE resistance measured using EIS at 0 V is therefore two to three times smaller than that observed during chronopotentiometry at currents above 20 A. It is possible this could be due to the significant congestion caused by the zero-gap configuration, such that liquid reactants and gaseous products must compete to arrive and depart on the same side of each electrode, thereby leading to an effective increase in resistance, which is consistent with previous theories [21]. One way to test this hypothesis would be to increase the pressure inside the ZGE, although it has been stated this has little effect on resistance [21,56], and in fact their overall efficiency can be slightly worse [1]. In any case, the test-station was not designed with this in mind.

For the FGE the situation is reversed, since the ohmic resistance predicted by Equation (6) is just 235 mΩ, whereas the figure measured by EIS at 0 V was 599 mΩ. It is possible this

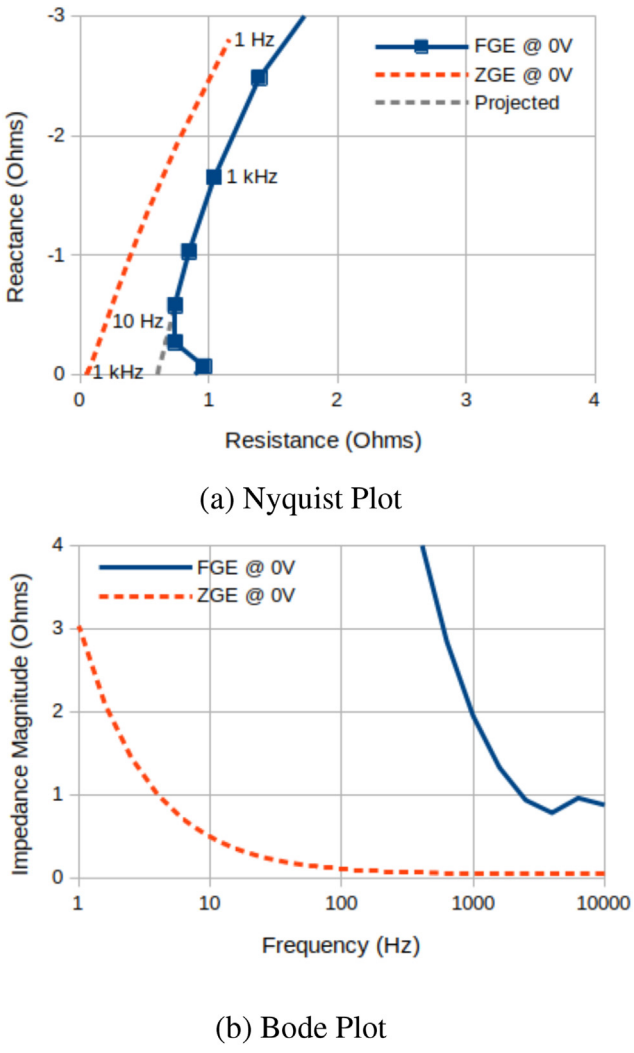

Fig. 7 – Electrochemical Impedance Spectroscopy (EIS) results for comparable finite-gap and zero-gap electrolysers. Configuration: 6-cells, bipolar. Electrolyte: 6 M KOH. Bias voltage: 0 V. Temperature: 293 K.

Table 3 – EIS measurements corresponding to the results in Fig. 7.

Configuration	Resistance mΩ	Capacitance mF	Area Resistance Ω cm^2 $cell^{-1}$
Finite-gap	599	0.6	4.9
Zero-gap	53	40	0.45

is because the surfaces of the plain 316SS electrodes had passivated sufficiently to become effectively open-circuit at the typical low voltages and currents employed during EIS. A further confounding factor is that the FGE is designed with four electrolyte side-channels that pass directly through the stack, and are thus able to provide a short-circuit at low current densities. This short-circuit disappears at high current densities, since the side-channels are unable to pass anywhere near the same amount of current as the electrodes.

The most striking feature of the EIS results is the large disparity between the frequency responses shown in Fig. 7(b). It is true that a higher capacitance should be expected for a ZGE, since the electrodes are only separated by the width of the membrane, however taking a magnitude of 2 Ω as a baseline the difference was in excess of 9 octaves. In retrospect, it is likely this is further evidence of the passivated nature of the plain 316SS electrodes in the FGE, since it implies they were able to change potential rapidly without the need to pass much electrical charge, which is indicative of electrical isolation.

Conclusions

The objective of this study is to provide sufficient information to guide design choices surrounding zero-gap electrolyser design. Not all electrolysers can be operated using the most conductive electrolyte, due to concerns surrounding safety and long-term corrosion resistance. Likewise, neither can all electrolysers be operated at temperatures above ambient, particularly if connected to intermittent renewable energy sources, where the cost of external heating is unjustifiable. Nevertheless, a virtuous circle exists whereby a less efficient electrolyser at low temperatures can be optimised to self-heat, and thus improve its own efficiency. It is for this reason that measurements at higher temperatures are included, since they inform self-heating electrolyser design.

Similarly, the quantitative electrolyser model presented in Section Model fitting permits the results from one size and shape of electrolyser to be projected onto another. With just three parameters (plus one fixed) the model is able to represent a sufficiently accurate simulation, at least at commercially significant current densities. This model is therefore adequate to guide electrolyser design given target efficiency and power capacity goals.

The effect of changing the membrane from Zirfon to PES was to introduce a voltage improvement of approximately 200 mV per cell. This is significant, since it occurred even at the highest current density, and with the most conductive electrolyte. However, since it is known that PES is a hydrophobic membrane, further work would be required to confirm that this extra performance did not come at the cost of increased gas mixing, specifically at the kind of lower current densities which can be typical of renewable energy applications.

Crucial to the performance of any zero-gap electrolyser is the design of the membrane electrode assembly, and specifically its electrical resistance. The design here presented is one of the cheapest and simplest it is possible to produce. The flowplate consists of off-the-shelf stainless steel materials, which are spot-welded together, and shaped largely using basic workshop tools. Similarly, the electrodes consist of woven stainless-steel mesh, onto which a simple two-stage Raney nickel coating is electrodeposited.

Even though stainless-steel is not the cheapest of metals, it is estimated that the materials for the six-cell electrolyser here presented could be purchased for less than 50 GBP (70 USD), and its construction involves zero machining costs. A version scaled up to 100 kW and an efficiency of 84% would have 24 plates and cost 3000 GBP (4000 USD). Should an efficiency of 75% prove acceptable, then the cost is halved. At a time when fossil fuel prices almost doubled in just 12 months, driving high levels of inflation,[3] and the prospect of war is forcing countries to regard dependence on fossil fuel as a threat to their national security,[4] it is clear that the case for renewable energy storage as hydrogen has never been stronger.

CRediT authorship contribution statement

William J F Gannon: Methodology, Software, Validation, Investigation, Writing. **Maximillian Newberry:** Investigation. **Charles W Dunnill:** Conceptualization, Supervision, Project administration, Funding acquisition.

Funding

This research was conducted as part of the DESIRE project, funded through the European Regional Development Fund via the Welsh Government [grant number SU213].

Declaration of competing interest

The authors declare that they have no known competing financial interests or personal relationships that could have appeared to influence the work reported in this paper.

Appendix A. Supplementary data

Supplementary data to this article can be found online at https://doi.org/10.1016/j.ijhydene.2022.07.040.

REFERENCES

[1] Abdin Z, Webb C, Gray E. Modelling and simulation of an alkaline electrolyser cell. Energy 2017;138:316–31. https://doi.org/10.1016/j.energy.2017.07.053. https://linkinghub.elsevier.com/retrieve/pii/S0360544217312288.

[2] American Iron and Steel Institute. Welding of stainless steels and other joining methods. Aisi; 1988. p. 1–46.

[3] Source: IMF https://blogs.imf.org/2022/01/28/viewed May 2022.

[4] Source: European Central Bank https://tinyurl.com/p4ue3zh2 viewed May 2022.

[3] Bachellerie E, Arnould F, Auglaire M, de Boeck B, Braillard O, Eckardt B, Ferroni F, Moffett R. Generic approach for designing and implementing a passive autocatalytic recombiner PAR-system in nuclear power plant containments. Nucl Eng Des 2003;221:151–65. https://doi.org/10.1016/S0029-5493(02)00330-8. https://linkinghub.elsevier.com/retrieve/pii/S0029549302003308.
[4] Blanchat TK, Malliakos A. Analysis of hydrogen depletion using a scaled passive autocatalytic recombiner. Nucl Eng Des 1999;187:229–39. https://doi.org/10.1016/S0029-5493(98)00283-0. https://linkinghub.elsevier.com/retrieve/pii/S0029549398002830.
[5] Bourasseau C, Guinot B. Hydrogen: a storage means for renewable energies'. In: Godula-Jopek A, editor. Hydrogen production. Wiley; 2015. p. 311–82.
[6] Chen S, Thind SS, Chen A. Nanostructured materials for water splitting - state of the art and future needs: a mini-review. Electrochem Commun 2016;63:10–7. https://doi.org/10.1016/j.elecom.2015.12.003.
[7] Colli AN, Girault HH, Battistel A. Non-precious electrodes for practical alkaline water electrolysis. Materials 2019;12:1336. https://doi.org/10.3390/ma12081336. https://www.mdpi.com/1996-1944/12/8/1336.
[8] David M, Ocampo-Martínez C, Sánchez-Peña R. Advances in alkaline water electrolyzers: a review. J Energy Storage 2019;23:392–403. https://doi.org/10.1016/j.est.2019.03.001.
[9] Dincer I, Acar C. Review and evaluation of hydrogen production methods for better sustainability. Int J Hydrogen Energy 2014;40:11094–111. https://doi.org/10.1016/j.ijhydene.2014.12.035.
[10] Douglas TG, Cruden A, Infield D. Development of an ambient temperature alkaline electrolyser for dynamic operation with renewable energy sources. Int J Hydrogen Energy 2013;38:723–39. https://doi.org/10.1016/j.ijhydene.2012.10.071.
[11] Gannon W, Jones D, Dunnill C. Enhanced lifetime cathode for alkaline electrolysis using standard commercial titanium nitride coatings. Processes 2019;7:112. https://doi.org/10.3390/pr7020112. http://www.mdpi.com/2227-9717/7/2/112.
[12] Gannon WJ, Dunnill CW. Raney Nickel 2.0: development of a high-performance bifunctional electrocatalyst. Electrochim Acta 2019;322:134687. https://doi.org/10.1016/j.electacta.2019.134687.
[13] Gannon WJ, Dunnill CW. Apparent disagreement between cyclic voltammetry and electrochemical impedance spectroscopy explained by time-domain simulation of constant phase elements. Int J Hydrogen Energy 2020a;45:22383–93. https://doi.org/10.1016/j.ijhydene.2020.06.029. https://linkinghub.elsevier.com/retrieve/pii/S0360319920321662.
[14] Gannon WJ, Dunnill CW. Materials coatings and enhanced characterisation for alkaline water-splitting devices. Ph.D. Thesis. Swansea. URL. https://cronfa.swan.ac.uk/Record/cronfa57775; 2020b.
[15] Gannon WJF, Dunnill CW. Study of activity and super-capacitance exhibited by bifunctional Raney 2.0 catalyst for alkaline water-splitting electrolysis. Hydrogen 2020c;2:1–17. https://doi.org/10.3390/hydrogen2010001.
[16] Gannon WJF, Warwick MEA, Dunnill CW. Woven stainless-steel mesh as a gas separation membrane for alkaline water-splitting electrolysis. Membranes 2020;10:109. https://doi.org/10.3390/membranes10050109. https://www.mdpi.com/2077-0375/10/5/109.
[17] Gao G, Chen W. Design challenges of wind turbine generators. 2009 IEEE Electrical Insulation Conference. EIC 2009;2009:146–52. https://doi.org/10.1109/EIC.2009.5166334.
[18] Gillespie MI, van der Merwe F, Kriek RJ. Performance evaluation of a membraneless divergent electrode-flow-through (DEFT) alkaline electrolyser based on optimisation of electrolytic flow and electrode gap. J Power Sources 2015;293:228–35. https://doi.org/10.1016/j.jpowsour.2015.05.077. http://linkinghub.elsevier.com/retrieve/pii/S0378775315009684.
[19] Gilliam R, Graydon J, Kirk D, Thorpe S. A review of specific conductivities of potassium hydroxide solutions for various concentrations and temperatures. Int J Hydrogen Energy 2007;32:359–64. https://doi.org/10.1016/j.ijhydene.2006.10.062. https://linkinghub.elsevier.com/retrieve/pii/S0360319906005428.
[20] Grigoriev SA, Fateev VN, Bessarabov DG, Millet P. Current status, research trends, and challenges in water electrolysis science and technology. Int J Hydrogen Energy 2020;45(49):26036–58. https://doi.org/10.1016/j.ijhydene.2020.03.109.
[21] de Groot MT, Vreman AW. Ohmic resistance in zero gap alkaline electrolysis with a Zirfon diaphragm. Electrochimica Acta 2021;369. https://doi.org/10.1016/j.electacta.2020.137684.
[22] Haverkort JW. Modeling and experiments of binary electrolytes in the presence of diffusion, migration, and electro-osmotic flow. Phys Rev Appl 2020;14:1. https://doi.org/10.1103/PhysRevApplied.14.044047.
[23] Haverkort JW, Rajaei H. Electro-osmotic flow and the limiting current in alkaline water electrolysis. J Power Sources Adv 2020;6:100034. https://doi.org/10.1016/j.powera.2020.100034.
[24] Haverkort JW, Rajaei H. Voltage losses in zero-gap alkaline water electrolysis. J Power Sources 2021;497:229864. https://doi.org/10.1016/j.jpowsour.2021.229864.
[25] Houf W, Schefer R. Predicting radiative heat fluxes and flammability envelopes from unintended releases of hydrogen. Int J Hydrogen Energy 2007;32:136–51. https://doi.org/10.1016/j.ijhydene.2006.04.009. https://linkinghub.elsevier.com/retrieve/pii/S0360319906001704.
[26] Jansson REW, Marshall RJ, Rizzo JE. The rotating electrolyser. I. The velocity field. J Appl Electrochem 1978;8:281–5. https://doi.org/10.1007/BF00612680.
[27] de Jonge R, Barendrecht E, Janssen L, van Stralen S. Gas bubble behaviour and electrolyte resistance during water electrolysis. Int J Hydrogen Energy 1982;7:883–94. https://doi.org/10.1016/0360-3199(82)90007-6. https://linkinghub.elsevier.com/retrieve/pii/0360319982900076.
[28] Jupudi RS, Zappi G, Bourgeois R. Prediction of shunt currents in a bipolar electrolyzer stack by difference calculus. J Appl Electrochem 2007;37:921–31. https://doi.org/10.1007/s10800-007-9330-4.
[29] Kuhn AT, Booth JS. Electrical leakage currents in bipolar cell stacks. J Appl Electrochem 1980;10:233–7. https://doi.org/10.1007/BF00726091. http://link.springer.com/10.1007/BF00726091.
[30] Liu Z, Sajjad SD, Gao Y, Yang H, Kaczur JJ, Masel RI. The effect of membrane on an alkaline water electrolyzer. Int J Hydrogen Energy 2017;42:29661–5. https://doi.org/10.1016/j.ijhydene.2017.10.050.
[31] Manabe A, Kashiwase M, Hashimoto T, Hayashida T, Kato A, Hirao K, Shimomura I, Nagashima I. Basic study of alkaline water electrolysis. Electrochim Acta 2013;100:249–56. https://doi.org/10.1016/j.electacta.2012.12.105.
[32] Mandin P, Derhoumi Z, Roustan H, Rolf W. Bubble over-potential during two-phase alkaline water electrolysis. Electrochim Acta 2014;128:248–58. https://doi.org/10.1016/j.electacta.2013.11.068.
[33] Mansilla C, Dautremont S, Shoai Tehrani B, Cotin G, Avril S, Burkhalter E. Reducing the hydrogen production cost by operating alkaline electrolysis as a discontinuous process in

the French market context. Int J Hydrogen Energy 2011;36:6407–13. https://doi.org/10.1016/j.ijhydene.2011.03.004.
[34] Motealleh B, Liu Z, Masel RI, Sculley JP, Richard Ni Z, Meroueh L. Next-generation anion exchange membrane water electrolyzers operating for commercially relevant lifetimes. Int J Hydrogen Energy 2021;46:3379–86. https://doi.org/10.1016/j.ijhydene.2020.10.244.
[35] Papadopoulos V, Desmet J, Knockaert J, Develder C. Improving the utilization factor of a PEM electrolyzer powered by a 15 MW PV park by combining wind power and battery storage – feasibility study. Int J Hydrogen Energy 2018;43:16468–78. https://doi.org/10.1016/j.ijhydene.2018.07.069.
[36] Passas G, Dunnill CW. Water splitting test cell for renewable energy storage as hydrogen gas. Fundam Renew Energy Appl 2015;5:3–8. https://doi.org/10.4172/2090-4541.1000188. https://tinyurl.com/3m78wvj5.
[37] Phillips R, Dunnill CW. Zero gap alkaline electrolysis cell design for renewable energy storage as hydrogen gas. RSC Adv 2016;6:100643–51. https://doi.org/10.1039/C6RA22242K. http://xlink.rsc.org/?DOI=C6RA22242K.
[38] Phillips R, Edwards A, Rome B, Jones DR, Dunnill CW. Minimising the ohmic resistance of an alkaline electrolysis cell through effective cell design. Int J Hydrogen Energy 2017;42:23986–94. https://doi.org/10.1016/j.ijhydene.2017.07.184. https://linkinghub.elsevier.com/retrieve/pii/S0360319917330203.
[39] Pletcher D, Li X. Prospects for alkaline zero gap water electrolysers for hydrogen production. Int J Hydrogen Energy 2011;36:15089–104. https://doi.org/10.1016/j.ijhydene.2011.08.080. https://linkinghub.elsevier.com/retrieve/pii/S0360319911020015.
[40] Preuster P, Papp C, Wasserscheid P. Liquid organic hydrogen carriers (LOHCs): toward a hydrogen-free hydrogen economy. Acc Chem Res 2017;50:74–85. https://doi.org/10.1021/acs.accounts.6b00474.
[41] Rearden A, Mandale S, Glover K, Phillips R, Dunnill CW. Optimizing the design of an alkaline water splitting device test cell for renewable energy storage as hydrogen. Arch Chem Chem Eng 2020;2.
[42] Rivard E, Trudeau M, Zaghib K. Hydrogen storage for mobility: a review. Materials 2019;12. https://doi.org/10.3390/ma12121973.
[43] Rodríguez Palmas, Sánchez-Molina Amores, Mais Campana. Simple and precise approach for determination of ohmic contribution of diaphragms in alkaline water electrolysis. Membranes 2019;9:129. https://doi.org/10.3390/membranes9100129. https://www.mdpi.com/2077-0375/9/10/129.
[44] Rousar I, Cezner V. Experimental determination and calculation of parasitic currents in bipolar electrolyzers with application to chlorate electrolyzer. J Electrochem Soc 1974;121:648–51.
[45] Schalenbach M, Kasian O, Mayrhofer KJ. An alkaline water electrolyzer with nickel electrodes enables efficient high current density operation. Int J Hydrogen Energy 2018;43:11932–8. https://doi.org/10.1016/j.ijhydene.2018.04.219.
[46] Shinagawa T, Garcia-Esparza AT, Takanabe K. Insight on Tafel slopes from a microkinetic analysis of aqueous electrocatalysis for energy conversion. Sci Rep 2015;5:13801. https://doi.org/10.1038/srep.13801. http://www.nature.com/articles/srep13801.
[47] Subramanian B, Ismail S. Production and use of HHO gas in IC engines. Int J Hydrogen Energy 2018;43:7140–54. https://doi.org/10.1016/j.ijhydene.2018.02.120.
[48] Tobias CW. Effect of gas evolution on current distribution and ohmic resistance in electrolyzers. J Electrochem Soc 1959;106:833. https://doi.org/10.1149/1.2427506.
[49] Ursúa A, Gandía LM, Sanchis P. Hydrogen production from water electrolysis: current status and future trends. Proc IEEE 2012;100:410–26. https://doi.org/10.1109/JPROC.2011.2156750.
[50] Ursúa A, San Martín I, Barrios EL, Sanchis P. Stand-alone operation of an alkaline water electrolyser fed by wind and photovoltaic systems. Int J Hydrogen Energy 2013;38:14952–67. https://doi.org/10.1016/j.ijhydene.2013.09.085. https://linkinghub.elsevier.com/retrieve/pii/S0360319913023082.
[51] Vermeiren P, Moreels JP, Leysen R. Porosity in composite Zirfon® membranes. J Porous Mater 1996;3:33–40. https://doi.org/10.1007/BF01135359.
[52] Wang G, Weng Y, Chu D, Chen R, Xie D. Developing a polysulfone-based alkaline anion exchange membrane for improved ionic conductivity. J Membr Sci 2009;332:63–8. https://doi.org/10.1016/j.memsci.2009.01.038.
[53] Weedy BM. The analogy between thermal and electrical quantities. Elec Power Syst Res 1988;15:197–201. https://doi.org/10.1016/0378-7796(88)90024-7.
[54] Wu Z, Li Z, Li H, Sun M, Han S, Cai C, Shen W, Fu Y. Ultrafast response/recovery and high selectivity of the H 2 S gas sensor based on α-Fe 2 O 3 nano-ellipsoids from one-step hydrothermal synthesis. ACS Appl Mater Interfaces 2019;11:12761–9. https://doi.org/10.1021/acsami.8b22517.
[55] Yu F, Li F, Sun L. Stainless steel as an efficient electrocatalyst for water oxidation in alkaline solution. Int J Hydrogen Energy 2016;41:5230–3. https://doi.org/10.1016/j.ijhydene.2016.01.108.
[56] Zeng K, Zhang D. Recent progress in alkaline water electrolysis for hydrogen production and applications. Prog Energy Combust Sci 2010;36:307–26. https://doi.org/10.1016/j.pecs.2009.11.002.